Proceedings of the Canadian Society for Mechanical Engineering International Congress
32nd Annual Conference of the Computational Fluid Dynamics Society of Canada
Canadian Society of Rheology Symposium
CSME/CFDSC/CSR 2025
May 25–28, 2025, Montréal, Québec, Canada

Automated 3D Propeller Modeling for Integration into a Shape Optimization Workflow

Irtiza M. Khan*, Finley M. Corbett, Tiger L. Jeans, Andrew G. Gerber, Juan A. Carretero
Department of Mechanical Engineering, University of New Brunswick, Fredericton NB, Canada
*irtiza.khan@unb.ca

***Abstract*—Marine propeller optimization is crucial for enhancing vehicle efficiency and minimizing environmental impact. This paper demonstrates developing a robust and automated 3D propeller modeling method which can be easily integrated into a shape optimization workflow using automated meshing and Reynolds-Averaged Navier-Stokes (RANS) solvers. The goal is to design high-performance propellers with improved efficiency and reduced cavitation. By leveraging high-fidelity 3D Computational Fluid Dynamics (CFD) simulations over low-order methods, the approach can enable better wake resolution, account for hull effects, and optimize propellers with retrofits. The paper demonstrates the automated modeling process, validates it with an existing propeller, and outlines the optimization workflow. Future efforts will focus on employing the methodology to modify existing propellers, perform multi-objective optimizations, and emphasize the role of high-fidelity CFD driven optimizations in advancing sustainable marine propulsion.**

***Keywords*—Marine propeller, propeller design, shape optimization, efficient propulsion.**

I. Introduction

Ships have been an essential part of transportation throughout human history. The international shipping industry is responsible for approximately 90% of global trade [1]. By the end of 2022, the world shipping fleet's deadweight tonnage had doubled compared to 2007 [2]. However, the increased usage of vessels has taken a significant environmental toll. A study from the International Marine Organization (IMO) showed that in 2018, greenhouse gas (GHG) emissions from shipping accounted for approximately 2.89% of global GHG emissions [3]. To reduce the environmental impact, the IMO Energy Efficiency Design Index (EEDI) and the Ship Energy Efficient Management Plan (SEEMP) went into effect in 2013 with more restrictions coming to reduce GHG emissions [4]. A highly efficient propulsion system can significantly improve fuel consumption and reduce GHG emissions. Bašić *et al.* [5] showed that propeller shape optimization using *PropSCAN* technology led to an approximately 1.41% drop in fuel consumption on a passenger ship, reducing CO_2 emissions by over 96 thousand tons annually. Cavitation inception is another significant consideration in propeller design and research has been conducted to mitigate cavitation inception during shape optimization [6].

Several different techniques have been employed for shape optimization. Typically, a propeller shape optimization process includes geometry parametrization, hydrodynamics performance evaluations, and optimization algorithms. Previously, low-order computational methods, such as Vortex Lattice Methods (VLM) and panel methods, were commonly used for their computational efficiency. Mishima *et al.* [7] parametrized propeller geometry using a cubic basic spline (B-spline) surface controlled by a four-by-four grid of control points. In this study, a VLM-based tool *HPUF-3A* was used along with a non-linear optimization method *CAVOPT-3D* to design cavitating propellers in nonuniform flow conditions.

With the increase in computational availability, Computational Fluid Dynamics (CFD) has become part of many optimization workflows to compute complex flows accurately. Cha *et al.* [8] used a combination of *HPUF-3A* and a Reynolds-Averaged Navier-Stokes (RANS) based solver to account for hull interaction while optimizing contra-rotating propellers. This approach has also been used to optimize ducted propellers [9]. Du *et al.* [10] designed an optimized propeller with winglets using an optimization algorithm called *SHERPA* and the RANS solver *STAR-CCM+*. According to unsteady RANS simulations, the optimized winglet design increased efficiency by 1 - 2% compared to conventional designs. Attaching retrofit energy-saving devices (ESD) such as propeller boss cap fins (PCBF) have also been considered

Natural Sciences and Engineering Research Council of Canada (NSERC)
Defence Research and Development Canada (DRDC)
Biome Renewables®

to improve propulsion efficiency. Gaggero [11] used a RANS solver along with a genetic algorithm to optimize two propeller models which showed improvement in efficiency under open-water conditions with the PCBF attached.

This paper focuses on developing an automated propeller geometry parametrization procedure capable of handling varying propeller shapes and creating a 3D propeller computer aided design (CAD) model. The goal is to integrate this method into an automated optimization workflow, which this paper will also briefly discuss. Furthermore, appropriate mesh and CFD setup for this workflow are presented.

II. Motivation and Overview of Workflow

Upon completion, this workflow will be employed to design an optimized propeller for the Royal Canadian Navy's ORCA class training vessels as a test case. The objective will be to attain a design that yields maximum efficiency under certain operating conditions while using cavitation as a constraint. In future, this workflow will be employed to perform multi-objective and multi-component optimization. In Fig. 1, the entire workflow is presented as a flowchart.

The process begins with providing initial design parameters to create a propeller geometry. Based on the data provided, the geometry is developed in two steps: 1) parametrization, and 2) generation of a 3D model using in-house developed tools *XBlade* and *XCAD* (described in section III). The watertight geometry is then meshed using an automated meshing script and used as the computational domain for a commercial RANS solver for CFD analysis. The performance metrics will then be used as inputs for an optimization algorithm to manipulate the design variables creating new models. Once the selected optimization criteria are met, the process stops and outputs a final propeller design.

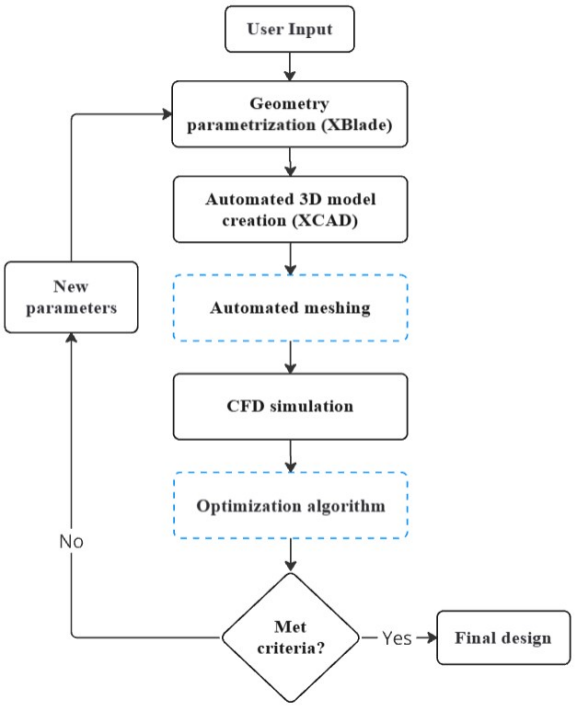

Figure. 1: Full workflow of the propeller shape optimization process. The blue boxes indicate steps which are still under development.

III. Geometry Creation

A. Parametrization Methodology

Appropriate geometry parametrization is the first step in shape optimization. An efficient parametrization process enhances the optimization workflow by improving accuracy, consistency, and usability. First, the parameters needed to describe propeller geometry are discussed. Generally, a propeller blade can be described as consisting of 2D airfoil cross-sections from the root to the tip. To fully define an airfoil, parameters include the camber distribution, thickness distribution, maximum thickness, maximum camber, and chord length. The design method described in this paper uses existing airfoils with defined camber and thickness distributions (*e.g.* NACA airfoils) which are used to create the 2D blade sections. The number of airfoils the user defines radially from the root to the tip correlates to the amount of control needed over the blade surface shape.

Once all the airfoils are parametrized, the next step is determining how they are stacked radially. Stacking airfoils densely in regions of high curvature is often necessary to accurately generate the blade surface. In this design method, the airfoils will be stacked at the midpoint of the chord line. It is common in propeller parametrization to define blade sections using a cylindrical coordinate system. The sections created through this design strategy conform to a cylindrical surface of the corresponding radii, as seen in Fig. 2. The parameters that define the orientation of these sections are pitch, skew angle, and rake. Although different definitions of pitch exist in the literature, here it is defined here as the angle between the chord line and the plane of rotation. Pitch can also be expressed as a distance which can be easily converted in terms of an angle angle and viceversa using,

$$\theta_{nt} = \tan^{-1} \frac{p}{2\pi r}, \tag{1}$$

where p is pitch distance, θ_{nt} is pitch angle, and r is the radial location of the blade section. The skew at a radial location

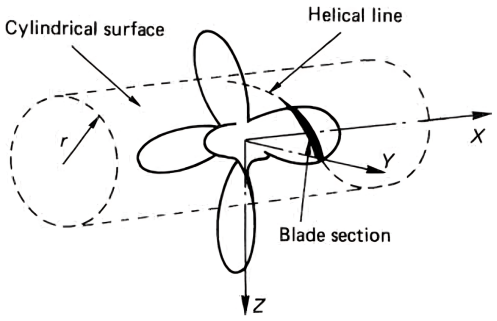

Figure. 2: Definitions of the global coordinate system and a cylindrical blade section at a radial location r. Picture taken from [12].

is defined as the angle between the propeller reference line and a line connecting the centre-point of the hub to the mid-chord of the airfoil. The propeller reference line is defined as a normal line drawn from the center of the hub along the Z-axis (referring to the same global coordinate system as in Fig. 2. Looking at the X-Z plane view from the same figure, the rake of a section is described as the distance between the mid-chord point of the root section and the mid-chord point of that section along the X-axis. Once the pitch, skew, and rake data are provided, all the necessary information to fully parametrize any blade section along the span is now available and the construction of the entire blade can begin. The 3D coordinates (in the global X-Y-Z reference frame shown in Fig. 2) of the lower and the upper surfaces of a section of the blade are calculated using:

$$x = -[i_G + r\theta_s \tan(\theta_{nt})] + (0.5c - x_c)\sin(\theta_{nt}) + y_{u,L}\cos(\theta_{nt}), \quad (2)$$

$$y = r\sin[\theta_s - \frac{180[(0.5c - x_c)\cos(\theta_{nt} - y_{u,L}\sin(\theta_{nt})]}{\pi r}], \quad (3)$$

$$z = r\cos[\theta_s - \frac{180[(0.5c - x_c)\cos(\theta_{nt} - y_{u,L}\sin(\theta_{nt})]}{\pi r}]. \quad (4)$$

In these equations, i_G is the rake, c is the chord length, and θ_s is the skew angle corresponding to that specific blade section. For any point along a nondimensional chord line, x_c is the distance along that line and $y_{u,L}$ are the y ordinates of the upper and the lower surfaces of an airfoil defined on a 2D Cartesian plane. A detailed explanation of these definitions and derivations of the equations can be found in [12].

Using (2) through (4), blade sections at any radial location can be generated. However, to generate the entire blade, an infinite number of blade sections from the root to the tip will need to be parametrized, in other words, continuous definitions of these parameters are required. To handle this, high order polynomials are fitted through discrete data points to prescribe continuous functions as demonstrated in Fig. 3a and Fig. 3b. This process enables efficient use of parameter data by clustering points near areas with rapid changes while reducing the number of data needed in areas with minimal change. Using these continuous functions, any number of blade sections can be defined along the span which provides the desired degrees of accuracy. As indicated in Fig. 1, this process is executed by an in-house developed tool *XBlade*. The input for this tool is the parameter data points and it outputs 3D coordinates of blade sections at the desired radial locations constructing a skeleton of the blade. The output can be then exported as a data file for CAD generation.

This process is demonstrated using the ORCA propeller No. 7836L [13]. The blades for the ORCA propeller consist of NACA 6-series airfoil profiles. Figure 3a and 3b show the available parameter data points. The x-axis is the nondimensional radius, R, spanning from 0 to 1 (root to tip of the blade). To maintain the confidentiality of the ORCA geometry, the y-axes have been redacted. A comparison between blade sections at one radial location is shown in Fig. 3c to demonstrate the accuracy of this tool. Figure. 4 shows a sample output from *XBlade* in the Y-Z planar view (as defined in Fig. 2).

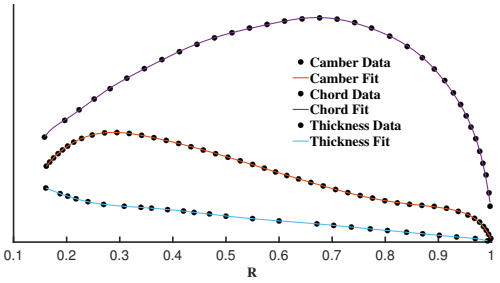

(a) Parameters which define the section shape.

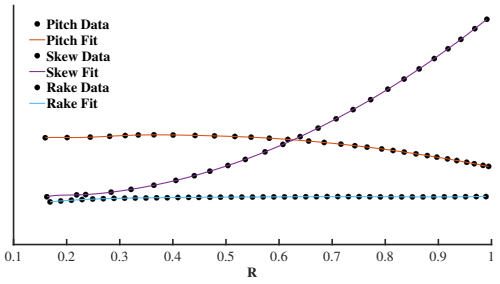

(b) Parameters which define how sections are stacked along the span of the blade.

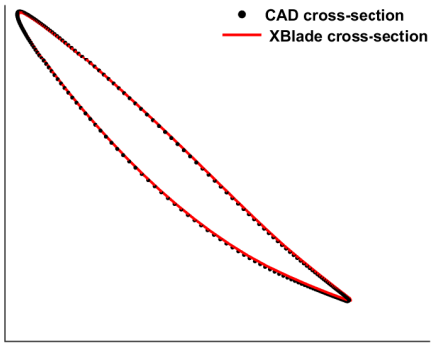

(c) A blade section extracted from the ORCA CAD model (received through private communications) is overlayed on the same section generated by *XBlade* at 0.3 R (nondimensional radius).

Figure. 3: Polynimial curve fits generated using the available data (not to scale). For validation, a comparison is shown at 0.3 R between a blade section extracted from original ORCA CAD model and a blade section generated using the polynomial curve fits.

B. Model Creation

The next step of the workflow is to create a solid propeller model that can be meshed and then analyzed by a RANS solver. Another tool called *XCAD* was built in-house to handle the automated 3D model creation step of the workflow (shown in Fig. 1). To construct the 3D model, the open-source CAD kernel Open CASCADE Technology (OCCT) is used. The OCCT library offers an expansive list of built-in functions accessible through programming languages such as C++ and Python (using the pythonOCC wrapper) to generate and manipulate CAD models.

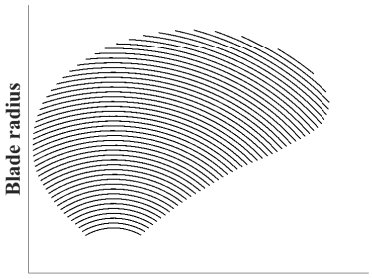

Figure. 4: Thirty blade sections constructing a skeleton of the ORCA propeller blade generated in *XBlade* (not to scale).

First, the data file generated in *XBlade* is read into the pythonOCC environment. Then, each blade section is approximated using basic-splines (B-Splines) fitted through their corresponding 3D coordinate points. Each section is described by two basic-splines: upper and lower curves. These geometric curves are then converted into topological edges with vertices at the end points. The upper and lower edges are then combined into a wire for each blade section which can be used in the OCCT environment to create surfaces. After that, continuous faces (surfaces) are generated by combining all the wires from the root to the tip. Fifth-order polynomial approximations are used to generate these smooth curved surfaces through all the sections. At the tip, the last section wire is patched with a curved face to created a closed watertight shell. A cylindrical hub is then created based on the hub radius and stitched to root blade section. This completes the CAD creation process for axisymmetric propellers (one blade is sufficient for CFD simulations using periodic boundary conditions). However, the full geometry can be generated by creating copies of the first blade and rotating them about the hub by a fixed amount. XCAD also allows for nonaxisymmetric propeller CAD generation, but it is not a part of this study. Models generated in the pythonOCC environment are then exported as STEP or IGES files and read into a meshing environment.

Once the *XBlade* and *XCAD* tools are connected, any propeller CAD model can be generated by prescribing all the necessary parameters. Figure 5 shows the ORCA propeller CAD model generated by the original polynomials, and some variations generated by modifying the polynomials.

These tools automate the model creation process, eliminating the manual intervention typically required to create CAD models. They are beneficial as propeller modeling tools and can be integrated into optimization workflows which use RANS solvers. The automated CAD generation enables an extensive search through the design space by efficiently producing the desired model variations in a short amount of time.

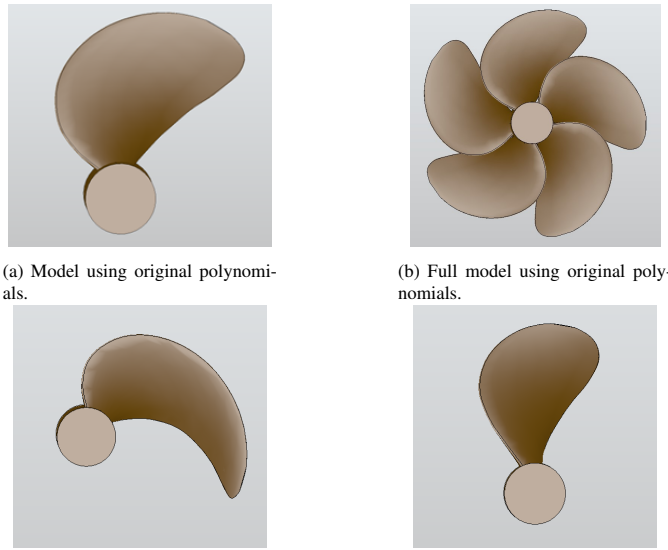

(a) Model using original polynomials.

(b) Full model using original polynomials.

(c) Model variation created with skew distribution scaled by a factor of two.

(d) Model variation created with pitch distribution scaled by a factor of two and skew distribution scaled to half of the original polynomials.

Figure. 5: Variations of the ORCA CAD models generated in *XCAD*.

IV. Mesh and CFD Setup

The next step is to analyze the developed CAD model and derive the necessary performance metrics for optimization. The automation of both meshing and CFD simulations is required for the optimization workflow shown in Fig. 1. In this section appropriate meshing and CFD setup strategies for the workflow are discussed using the ORCA propeller. Results of a preliminary mesh sensitivity study are also presented.

A. Mesh Setup

For meshing, the commercial software *Fidelity Pointwise* has been chosen which offers automated mesh scripting features. The mesh presented in this paper was created manually and will be scripted to automate mesh generation for new blade variations during optimization. Taking advantage of the periodicity of the ORCA propeller a periodic domain was created to limit the mesh size. The mesh setup is shown in Fig. 6.

As the propeller consists of five blades, the periodic domain is a 72-degree slice of the full rotor. To limit mesh complexity and maintain adequate flow field resolution, a hybrid mesh topology is employed. This involves refining the wake and boundary layer regions with structured hexahedra and using unstructured Delauney elements to transition to the farfield. The periodic boundaries are structured as curved planes to conform to the highly skewed blade geometry. The mesh was validated by completing CFD simulations and comparing to available experimental results over a range of advance ratios (J) near the operating conditions. A preliminary mesh sensitivity study was also performed to ensure that all the critical resolutions are kept while reducing simulation time (see Fig. 8).

B. CFD Setup

For CFD simulations, the commercial solver *Ansys CFX* is used. The CFD simulations will be automated by running them in batch from the command line. The CFD domain

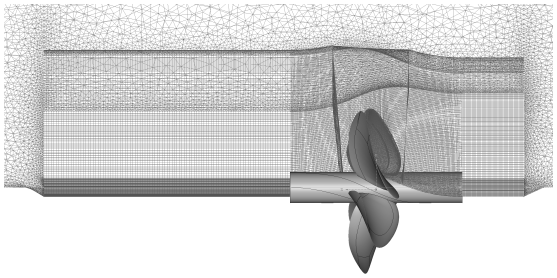

(a) Structured blocks around the blade.

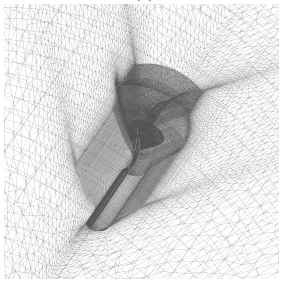

(b) Curved boundaries adjacent to the blade.

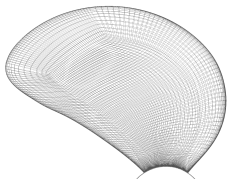

(c) Surface mesh.

Figure. 6: Variations of the ORCA propeller generated in *XCAD*.

and boundary conditions are shown in Fig. 7. All simulations conducted are steady state and use the $k-\omega$ Shear Stress Transport (SST) turbulence model. To model the rotating component of the propeller, *Frozen Rotor* interfaces are used to transition between the stationary and rotating domains.

The relevant performance metrics are torque coefficient (K_Q), thrust coefficient (K_T), and open-water propeller efficiency (η). Traditionally, these metrics are plotted against the advance ratio (J) of the propeller. They are collectively defined as

$$K_T = \frac{T}{\rho n^2 D^4}, \tag{5}$$

$$K_Q = \frac{Q}{\rho n^2 D^5}, \tag{6}$$

$$\eta = \frac{K_T J}{K_Q 2\pi}, \tag{7}$$

$$J = \frac{V}{nD}, \tag{8}$$

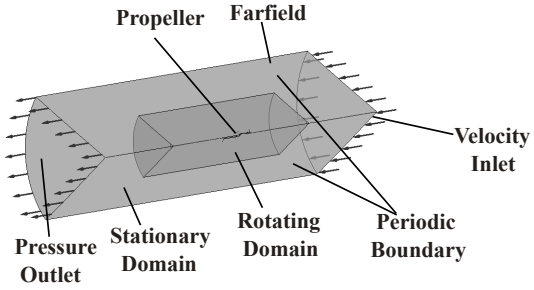

Figure. 7: CFD setup showing the boundary conditions and the fluid volumes in *Ansys CFX*.

where T is thrust, Q is torque. ρ is the density of the fluid, n is the propeller's rotational speed, D is the propeller's diameter, and V is the velocity of the free-stream flow.

C. Results

A preliminary mesh sensitivity study used wall y^+ and near-wake refinement as variables. Table I shows the cell counts, average wall y^+ and decay rate (refinement level of inflation layer transition to unstructured cells). In Mesh 1, the boundary layer was not resolved, resulting in a y^+ value over 70. For Mesh 2, 3, and 4, the boundary layer was resolved using structured growth layers near the blade surface. Figure 8 shows that wall y^+ has a noticeable impact on efficiency. Figure 9 visualizes the wake for Mesh 3 and Mesh 4 using isosurfaces created with vorticity magnitude at $50s^{-1}$. Due to less mesh refinement in the wake region, Mesh 3 showed more wake diffusion compared to Mesh 4. However, better wake resolution did not have any significant influence on the hydrodynamic loads as seen in Fig. 8. Therefore, Mesh 3 was chosen over Mesh 4.

Performance metrics were then compared to available experimental data to validate Mesh 3. The comparison was done over a range of J ($0.6 \leq J \leq 0.8$). The results showed $2.8-3.7\%$ difference in η values between simulations and

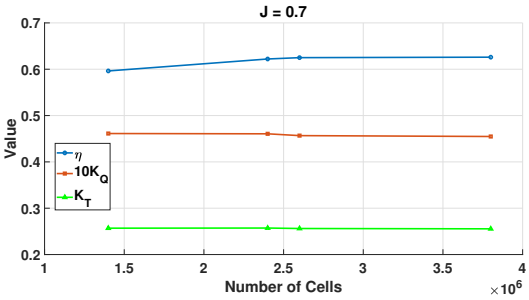

Figure. 8: Results of mesh sensitivity analysis comparing performance metrics among different mesh setups.

TABLE. I: Results of mesh sensitivity study

Mesh	Cell Count	Average y^+	Decay Rate
1	1.4E6	70	0.5
2	2.4E6	5	0.5
3	2.6E6	1	0.5
4	3.8E6	1	0.99

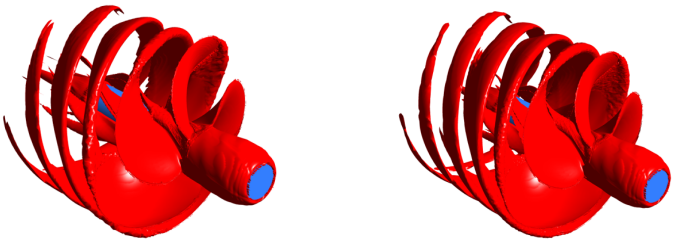

(a) Mesh 3.

(b) Mesh 4.

Figure. 9: Wake visualization by generating isosurfaces using vorticity magnitude at 50 s^{-1}.

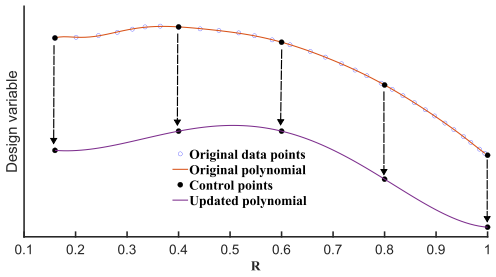

Figure. 10: New polynomials generated by manipulating control points.

experiments. Considering experimental uncertainties, Mesh 3 was accepted as a valid setup for the optimization.

V. Optimization Strategy

Considering that the optimization will have a large number of design variables, and that computing the gradient of the objective function will not be possible in reasonable time, a heuristic population-based optimization strategy will be used. The workflow will start with the initial geometry defined in the parametrization process. Then a number of control points will be perturbed for each parameter (*e.g.* pitch, skew, *etc.*) which will modify the original polynomials as shown in Fig. 10; a comparable approach was used in [7] where control points were used to manipulate a four-by-four grid that generates 2D blade surfaces. These control points are the design variables in this optimization. Based on the newly generated polynomials new variations of the propeller model will be automatically created for evaluation. Using less control points can reduce the optimization time but it does limit the amount of control over polynomial modifications. These control points are allowed to move independently only in the y-direction with predefined x-positions to further limit the optimization time.

Initially, to limit the search space to a reasonable size, the airfoil profile, *e.g.*, NACA 6-series, as well as the blade and hub radius, will not be modified during the optimization. Instead, only the parameters shown in Fig. 3a, and Fig. 3b will be varied using control points to arrive at a final design.

VI. Conclusion And Future Work

The long-term goal of this research is to develop a high-fidelity shape optimization process for designing marine propellers. This paper demonstrates a methodology to automate marine propeller modeling. Tools such *XBlade* and *XCAD* were developed in-house to facilitate this automation which can be integrated into an shape optimization workflow as shown in Fig. 1. Based on spanwise definitions for maximum camber, chord length, maximum thickness, pitch, skew, and rake, *XBlade* generates a series of stacked airfoil cross-sections representing the blade geometry. *XCAD* then utilizes these cross-sections to generate a solid watertight 3D CAD model using the open-source CAD kernel Open CASCADE. A variety of propeller shapes are generated (Fig. 5) to show the viability of the methodology.

The benefit of automated 3D modeling is that it facilitates using RANS solvers, like *Ansys CFX*, in the workflow instead of lower fidelity computational methods. A reasonable mesh size for optimizing the ORCA propeller is also explored (Fig. 8) with the intention of automating the mesh generation process.

Future work for this project is to finish automating the meshing process, integrate a population-based algorithm into the workflow, and then utilize this workflow to modify an optimized design of the ORCA propeller. Further developments will include multi-objective optimization, integration of hull effects, and multi-component optimization.

VII. Acknowledgements

The authors gratefully acknowledge the support provided by the Natural Sciences and Engineering Research Council of Canada (NSERC), Defence Research and Development Canada (DRDC), and Biome Renewables®. This work was made possible through funding provided by an alliance agreement and benefited significantly from the valuable data and expert advice contributed by these organizations.

References

[1] International Chamber of Shipping (ICS), "Shipping and world trade: World seaborne trade," https://www.ics-shipping.org/shipping-fact/shipping-and-world-trade-world-seaborne-trade/, 2025, accessed: 2025-01-15.

[2] Hellenic Shipping News, "Shipping fleet statistics 2022," https://www.hellenicshippingnews.com/shipping-fleet-statistics-2022/, 2025, accessed: 2025-01-15.

[3] International Maritime Organization (IMO), "2023 imo strategy on reduction of ghg emissions from ships," Marine Environment Protection Committee, London, UK, Tech. Rep. MEPC.377(80), Jul. 2023, adopted on 7 July 2023, Annex 15, MEPC 80/17/Add.1.

[4] ——, "Improving the energy efficiency of ships," https://www.imo.org/en/OurWork/Environment/Pages/Improving%20the%20energy%20efficiency%20of%20ships.aspx, 2025, accessed: 2025-01-24.

[5] B. Bacalja Bašić, M. Krčum, and Z. Jurić, "Propeller optimization in marine power systems: Exploring its contribution and correlation with renewable energy solutions," *Journal of Marine Science and Engineering*, vol. 12, no. 5, 2024.

[6] B. Epps, O. Viquez, and C. Chryssostomidis, "A method for propeller blade optimization and cavitation inception mitigation," *Journal of Ship Production and Design*, vol. 31, no. 2, pp. 88–99, 2015.

[7] S. Mishima and S. A. Kinnas, "Application of a numerical optimization technique to the design of cavitating propellers in nonuniform flow," *Journal of Ship Research*, vol. 41, no. 02, pp. 93–107, 06 1997.

[8] K. Cha and S. A. Kinnas, "An iterative non-linear optimization method for the design of contra-rotating propellers for an underwater vehicle," in *Proceedings of the 35th Symposium on Naval Hydrodynamics*, Nantes, France, Jul. 2024, held 8–12 July 2024.

[9] W. Du and S. Kinnas, "Optimization design and analysis of marine ducted propellers by rans/potential flow coupling method," in *Proceedings of the 29th International Ocean and Polar Engineering Conference*, 06 2019.

[10] W. Du, A. Gunderson, J. Reifsnyder, and K. Farrell, "Design, analysis and test of conventional and winglet propellers under highly loaded conditions," *Ocean Engineering*, vol. 284, p. 115173, 2023.

[11] S. Gaggero, "Design of pbcf energy saving devices using optimization strategies: A step towards a complete viscous design approach," *Ocean Engineering*, vol. 159, pp. 517–538, 2018.

[12] "Chapter 3 - propeller geometry," in *Marine Propellers and Propulsion (Fourth Edition)*, fourth edition ed., J. Carlton, Ed. Butterworth-Heinemann, 2019, pp. 29–46.

[13] G.-J. Zondervan and M. Merkins, "Orca class patrol vessels: Design and evaluation of new propellers," Defence Research and Development Canada (DRDC), Canada, Tech. Rep. DRDC-RDDC-2023-C028, Jan. 2023.